Million-fold sensitivity enhancement in proteopathic seed amplification assays for biospecimens by Hofmeister ion comparisons

Michael A. Metrick II[a,b], Natalia do Carmo Ferreira[a], Eri Saijo[a], Andrew G. Hughson[a], Allison Kraus[a], Christina Orrú[a], Michael W. Miller[c], Gianluigi Zanusso[d], Bernardino Ghetti[e], Michele Vendruscolo[b], and Byron Caughey[a,1]

[a]Laboratory of Persistent Viral Diseases, Rocky Mountain Laboratories, National Institute of Allergy and Infectious Diseases, NIH, Hamilton, MT 59840; [b]Centre for Misfolding Diseases, Department of Chemistry, University of Cambridge, Cambridge CB2 1EW, United Kingdom; [c]Colorado Division of Parks and Wildlife, Wildlife Health Program, Fort Collins, CO 80521-1049; [d]Department of Neurosciences, University of Verona, 37129 Verona, Italy; and [e]Department of Pathology and Laboratory Medicine, Indiana University School of Medicine, Indianapolis, IN 46202

Edited by Edward A. Hoover, Colorado State University, Fort Collins, CO, and approved September 24, 2019 (received for review June 14, 2019)

Recent work with prion diseases and synucleinopathies indicates that accurate diagnostic methods for protein-folding diseases can be based on the ultrasensitive, amplified measurement of pathological aggregates in biospecimens. A better understanding of the physicochemical factors that control the seeded polymerization of such aggregates, and their amplification in vitro, should allow improvements in existing assay platforms, as well as the development of new assays for other proteopathic aggregates. Here, we systematically investigated the effects of the ionic environment on the polymerization of tau, α-synuclein, and the prion protein (PrP) induced by aggregates in biospecimens. We screened salts of the Hofmeister series, a relative ordering of strongly and weakly hydrated salts that tend to precipitate or solubilize proteins. We found that sensitivities of tau-based assays for Alzheimer's seeds and PrP-based assays for prions were best in weakly hydrated anions. In contrast, we saw an inverse trend with different tau-based assays, improving detection sensitivity for progressive supranuclear palsy seeds by $\approx 10^6$. Hofmeister analysis also improved detection of sporadic Creutzfeldt–Jakob disease prions in human nasal brushings and chronic wasting disease prions in deer-ear homogenates. Our results demonstrate strong and divergent influences of ionic environments on the amplification and detection of proteopathic seeds as biomarkers for protein-folding diseases.

RT-QuIC | Hofmeister series | tau | ion hydration | protein misfolding

Neurodegenerative diseases are often difficult to diagnose early in the clinical phase (1), at least in part due to the lack of disease-specific biomarkers that are present in high enough concentrations to be detectable in accessible ante mortem diagnostic specimens. Consequently, definitive diagnosis of many neurodegenerative diseases relies on postmortem examination of brain pathology. Since many of these diseases result from the pathological misfolding and aggregation of native proteins into abnormal deposits, which can then act as templates to accelerate the recruitment of additional protein monomers (2–4), one promising route to developing effective diagnostic methods is to exploit this proliferation process to enhance the sensitivity of the detection.

To implement this strategy, we and others have developed prototypic amplification assays for several types of protein aggregates that can serve as disease biomarkers (5–11). In these assays, a biospecimen (e.g., brain homogenate [BH], cerebrospinal fluid [CSF], or nasal brushings) containing as little as attogram amounts of the protein aggregates to be detected is added to a mixture containing a vast excess of the corresponding protein monomer (the substrate) that can build onto the seed. Through this seeded polymerization process, the aggregates can be amplified by many orders of magnitude and detected with amyloid-sensitive fluorescent dyes, such as thioflavin T (ThT). In this context, we have developed several real-time quaking-induced conversion (RT-QuIC) assays for various protein-misfolding disorders, including prion diseases using CSF (8, 9), nasal brushings (12, 13), and skin (14); Parkinson's disease and diffuse Lewy body dementia (DLBD) using CSF and BH (6, 7); and Alzheimer's disease (AD) and Pick's disease (PiD) using BH (10, 15). These initial findings have highlighted the utility of seeded amplification assays for detecting protein aggregates of neurodegenerative diseases as biomarkers.

Generally, the development of a seeded amplification assay hinges on finding reaction conditions that both promote rapid propagation of amyloid from seeds in disease specimens and delay the spontaneous aggregation of the substrate protein in the mock-seeded reactions used as controls. Influential parameters include the substrate protein sequence, shaking speed, temperature, beads, salt concentration, and presence of cofactors and detergents (16).

Given the importance of the physico-chemical properties of a protein solution in the aggregation process—in particular, hydrophobicity and electrostatic charge (17)—we investigated the effects of modulating ionic composition on the efficiency of

Significance

Detection of aggregated proteins in human tissues represents a challenging, yet proven, avenue for diagnosing neurodegenerative diseases. For therapeutic advances to occur, an accurate and early diagnosis must be made, which would ideally rely on a biomarker that can track the progression of the disease. One challenging aspect to this approach is achieving enough sensitivity to detect very low (sometimes attogram, 10^{-18} g) amounts of aggregates in diagnostically available tissues. Here, we show that this level of sensitivity can be achieved through optimization of the ionic environment in which these aggregates are amplified through their self-seeding ability. The use of weakly or strongly hydrated anions can enhance the seeded-polymerization-based detection of aggregates from biological tissues, thus potentially enhancing the diagnostic capability of these assays.

Author contributions: M.A.M., N.d.C.F., E.S., M.V., and B.C. designed research; M.A.M., N.d.C.F., E.S., A.G.H., A.K., C.O., and B.G. performed research; M.A.M., N.d.C.F., E.S., A.G.H., A.K., C.O., M.W.M., G.Z., and B.G. contributed new reagents/analytic tools; M.A.M., N.d.C.F., E.S., A.G.H., A.K., C.O., M.W.M., G.Z., B.G., M.V., and B.C. analyzed data; and M.A.M., N.d.C.F., E.S., M.V., and B.C. wrote the paper.

Competing interest statement: M.A.M., E.S., A.K., and B.C. are inventors on a pending patent (US Application No. PCT/US2017/069024).

This article is a PNAS Direct Submission.

See Commentary on page 22894.

[1]To whom correspondence may be addressed. Email: bcaughey@nih.gov.

This article contains supporting information online at www.pnas.org/lookup/suppl/doi:10.1073/pnas.1909322116/-/DCSupplemental.

First published October 22, 2019.

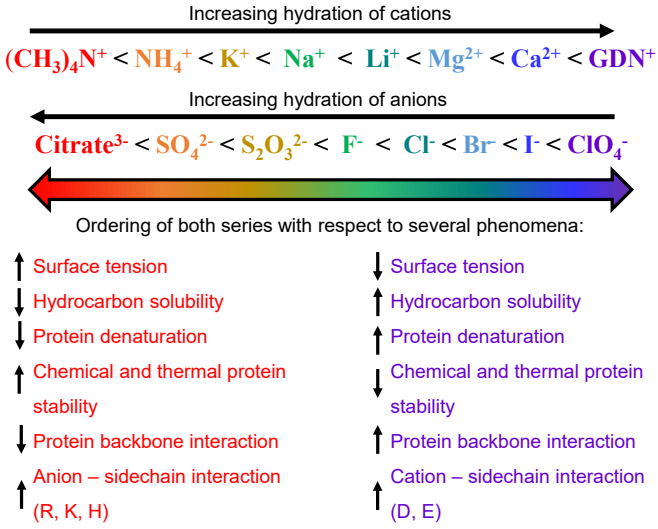

Fig. 1. Cationic and anionic Hofmeister series. The ion-hydration series is shown by black arrows, and the corresponding global biological and physical phenomena are listed. R, arginine; K, lysine; H, histidine; D, aspartate; E, glutamate. Adapted from ref. 21. Copyright (2006), with permission from Elsevier.

biospecimen-seeded polymerization. Most published RT-QuIC assays use sodium chloride (NaCl) as the main source of ionic components (6, 11, 16, 18, 19). To explore potentially more favorable salts, we started from Hofmeister's original observations of a series of anions and cations and their relative abilities to salt proteins out of solution (20). Since then, the relative ordering of anions and cations as they behave with regard to several physico-chemical phenomena related to protein solubility (or lack thereof) has been well established (Fig. 1) (21, 22). Attention has long focused, in particular, on the ability of ions to alter the properties of water, with kosmotropes having the ability to create water-molecule patterns and chaotropes to disrupt hydrogen-bonding networks between water molecules. Recent studies also indicate that other factors should be considered in interpreting the influences of the Hofmeister series of salts (23). Relevant physico-chemical properties influenced by the series include protein thermal stability (24), polymer solubility (25), water-surface tension (26), and patterning of water at the air–water interface (27). Indeed, the behaviors of some amyloid-forming proteins, including PrP (28), α-synuclein (α-Syn) (29), and the yeast prion-forming protein Sup35 (30), have been studied in the Hofmeister salt series. However, Hofmeister effects have not been investigated systematically in the context of polymerization reactions seeded by natural disease-associated protein aggregates.

Here, we report strikingly divergent ion effects on protein aggregation caused by different disease-associated seeds and their practical consequences in terms of optimizing seed-amplification biomarker assays of biospecimens. We tested Hofmeister salts in several RT-QuIC assays for pathological forms of tau (10, 15), α-Syn (7), and PrP (31, 32). We considered 4 key parameters for seeded-polymerization assays: sensitivity, fidelity, speed, and specificity (Table 1). We applied this optimization process in the development of a tau-seeding assay for neurodegenerative diseases involving the preferential accumulation of tau isoforms with 4-microtubule binding domains (4R tau molecules). We also investigated how altering the ionic environment of RT-QuIC reactions can facilitate diagnostics development by overcoming matrix effects from inhibition by unknown components in complex biospecimens, such as plasma, ear homogenates, and nasal brushings.

Results

Systematic Investigation of Ion Effects on AD Tau RT-QuIC. Using the RT-QuIC platform (*SI Appendix*, Fig. S1), we first compared effects of conducting the AD tau RT-QuIC (*SI Appendix*, Table S2) in the presence of strongly (citrate^{3-}), moderately (Cl^-), or weakly (I^-) hydrated anions at a concentration of 400 mM (Fig. 2), which was the optimal concentration for NaCl in our original AD RT-QuIC assay (15). Representative raw ThT fluorescence data over time for reactions with indicated dilutions of tau-free knockout (KO) mouse BH or AD BH (in 0.5% KO BH) are shown in Fig. 2*A*. Lag times (Fig. 2*B*) were calculated by setting a threshold of 100 SDs above the baseline ThT fluorescence and determining the time of the first ThT reading above such threshold. This analysis revealed rapid fibrillization in both mock-seeded (KO) and AD-seeded wells in Na_3Citrate, thus failing to generate any distinction in lag times (Fig. 2*B*). In contrast, much slower and less frequent mock-seeded fibrillization was seen by using NaCl and NaI, with shorter mean AD-seeded lag times, even with the most extreme end-point dilutions (10^{-8} to 10^{-10}) of AD BH. Calculation of the fold separation in mean lag times between AD- and KO-seeded reactions again indicated that NaCl and NaI, but not Na_3Citrate, allowed discrimination down to 10^{-8} and 10^{-10} AD BH, respectively (Fig. 2*C*). In general, ions toward the right sides of both the anionic and cationic series (i.e., weakly hydrated anions and strongly hydrated cations) delayed mock-seeded (KO only) fibrillization of τ306–378, without affecting significantly the kinetics of fibril formation in AD-seeded reactions with respect to NaCl (Fig. 2 and *SI Appendix*, Figs. S2–S4).

The Anionic Series Exerted Distinct Lag-Phase Effects on Prion, αSyn, and Tau RT-QuIC Assays. Experiments with 6 different RT-QuIC assays revealed distinct trends in the ordering of Hofmeister anion effects. Fig. 3 summarizes lag-phase data of recombinant Ha90 PrP seeded with hamster scrapie BH; K23Q αSyn seeded with DLBD BH; and K19CFh tau seeded with PiD BH. The Ha90 PrP lag-time plots showed a lack of ThT-positive fibril formation in strongly hydrated anions (Na_3Citrate and Na_2SO_4)

Table 1. Parameters considered during the optimization of RT-QuIC assays

Parameter	Definition	Measure	Salt effect
Sensitivity	Log_{10} dilution at which 50% of wells are positive	$logSD_{50}$	Up to a million-fold increase (Fig. 5; Table 2)
Fidelity	Kinetic separation of true positive from false positive reactions	Fold separation ($T_{lag\text{-}KO}/T_{lag}$, where T_{lag} is the lag time)	Up to 17-fold increase (Figs. 4, 7, and 8 and *SI Appendix*, Figs. S6–S9)
Speed	Characteristic time of aggregation	Lag time (hours)	Greater than 10-fold increase (Fig. 6*A*)
Specificity	Seeding from on-target disease sample, with no seeding from off-target sample	$logSD_{50}$ on-target minus $logSD_{50}$ off-target	Up to 5 log increase (Fig. 5)

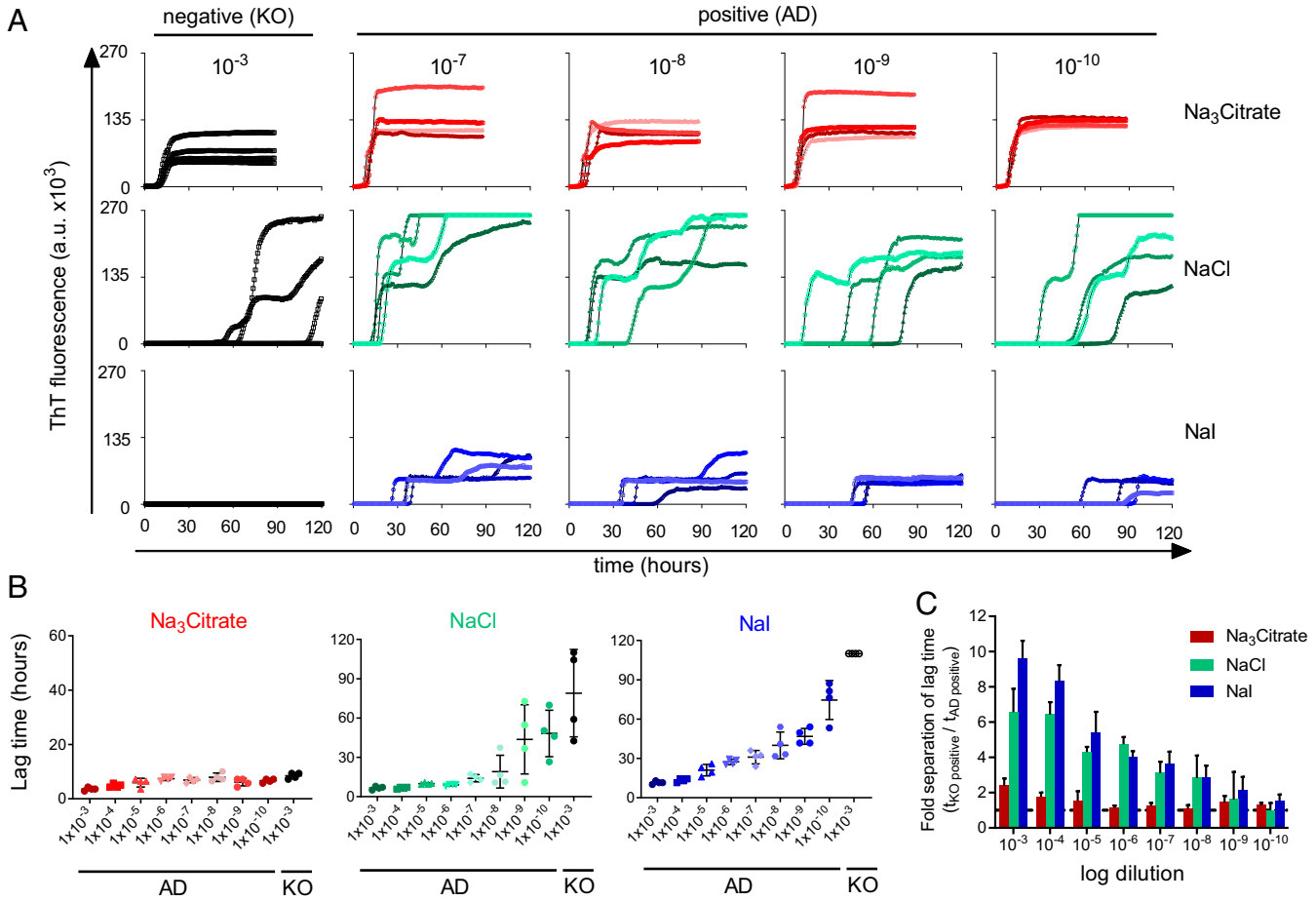

Fig. 2. Comparison of the effects of different salts in the Hofmeister series on the speed of the AD RT-QuIC assays. (*A*) Raw ThT fluorescence data of quadruplicate brain dilutions at 10^{-3} for KO (black) and 10^{-7} to 10^{-10} for AD brains (color) for a representative strongly hydrated anion ($Na_3Citrate$; red), neutral anion (NaCl; green), and weakly hydrated anion (NaI; blue). a.u., absorbance units. (*B*) Speed analysis (in terms of lag times) of the 3 salts represented in *A*; lag times were determined by setting a threshold value at 100 × SD of baseline fluorescence; bars represent the mean and SD of 4 replicate reactions, and gray dashed lines represent the time of the first spontaneous (KO-seeded) fibril reaching threshold. (*C*) Fold separation of lag times between positive and negative reactions, defined by $t_{false\ positive}/t_{true\ positive}$ or $t_{KO\ positive}/t_{AD\ positive}$; larger numbers represent greater separation; dashed line shows where fold separation is <1, meaning no discrimination between a true and false positive. Assays in the presence of different salts in the Hofmeister series differ in speed by up to a factor of 10.

within 60 h. By contrast, with more weakly hydrated anions, prion-seeded reactions were accelerated without commensurate acceleration in normal BH (NBH) mock-seeded reactions. αSyn RT-QuIC showed a bimodal distribution of DLBD-seeded fibril-formation rates (compare colored points left to right), where DLBD-seeded lag times were fastest at the ends of the anionic series; however, the lag times of mock-seeded fibril formation were delayed with decreasing ion hydration from 20 to >60 h, with the exception of NaF (compare black points left to right). Finally, in contrast to the prion RT-QuIC trend, PiD-seeded K19CFh tau fibrillization was fastest with more strongly hydrated anions, while weakly hydrated anions completely inhibited fibril formation in even the PiD dilutions containing the most seeds.

To normalize and summarize the Hofmeister effects on the different types of RT-QuIC assays, we plotted the fold separation between lag times of disease-seeded (true positive) fibril formation relative to mock-seeded (false positive) fibril formation as a function of BH dilution in Fig. 4. Fig. 4 *A*–*C* show data for the AD, bank vole (BV) PrP–prion, and Ha90 PrP–prion RT-QuIC reactions. Higher bars represent either an acceleration of seeded versus mock-seeded fibril formation, a delay of mock-seeded fibril formation, or a combination of the 2. These 3 assays showed clear enhancements of assay fidelity (8- to 11-fold) in weakly hydrated anions compared to strongly hydrated ones, with a general trend of citrate^{3-} < SO_4^{2-} < F^- < $S_2O_3^{2-}$ < Cl^- < Br^- < ClO_4^- ≈ I^-. In contrast, 3 additional assays for 3R tauopathy (PiD), 4R tauopathy (progressive supranuclear palsy [PSP]), and α-synucleinopathy (DLBD) showed inverse or bimodal trends. Fig. 4 *D* and *E* show the enhancement of fold separation in the K19-PiD and K18+K19-PSP assays in strongly hydrated anions and inhibition in weakly hydrated anions. Consistent with previous studies of Hofmeister effects on αSyn fibril elongation (29), we found that in the DLBD-seeded RT-QuIC assay, the shorter lag times were obtained at the extreme ends of the series (as depicted in Fig. 3), giving a bimodal distribution of fold separations in which SO_4^{2-} > $S_2O_3^{2-}$ > F^- < Cl^- ≈ Br^- ≈ I^- < ClO_4^-.

Hofmeister Effects on the Sensitivity of RT-QuIC Assays. To directly examine Hofmeister series effects on assay sensitivity, we used the Spearman–Kärber algorithm to calculate relative concentration of seeding units measured in a given BH using different assay permutations (33). We define an SD_{50} as a seeding unit giving 50% positive replicate reactions prior to a predetermined assay cutoff time set to be before ThT positivity in mock-seeded negative control reactions. Table 2 shows log SD_{50}

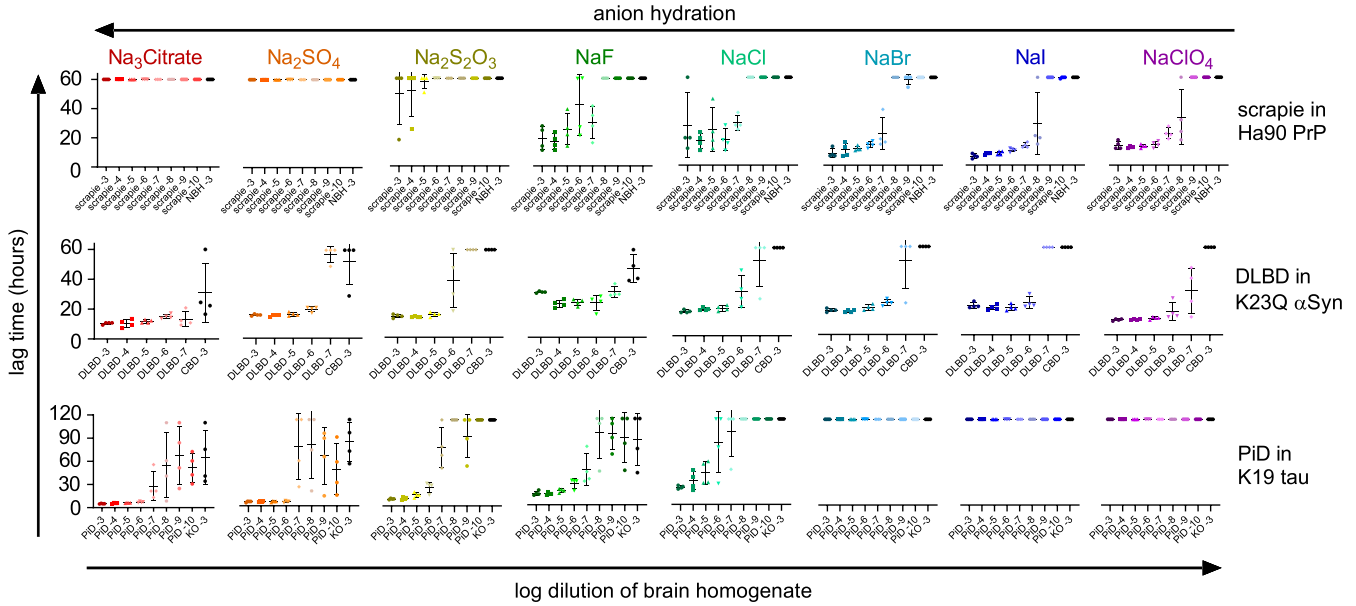

Fig. 3. Lag-phase analysis reveals 3 primary trends in the anionic Hofmeister series. Each point represents the time to threshold (100 × SD of baseline fluorescence) for a single reaction; positive reactions are shown in color on the left of each graph, while negative controls are shown in black. Bars represent the mean and SD of quadruplicate reactions.

concentrations per milligram of brain as measured in the Hofmeister series of anions. Darker blue shading indicates higher sensitivity, while the darker red shading indicates lower sensitivity. The heatmap is a relative representation of increased or decreased sensitivity within an assay; that is, the least sensitive salt in the AD assay (NaF) shares its shading with the least sensitive salts in the Ha90 prion assay—for example, $Na_3Citrate$ and Na_2SO_4—despite differing actual values. As expected, for each type of assay, the relative sensitivity trends (Table 2) generally followed the trends in fold separation shown in Fig. 4.

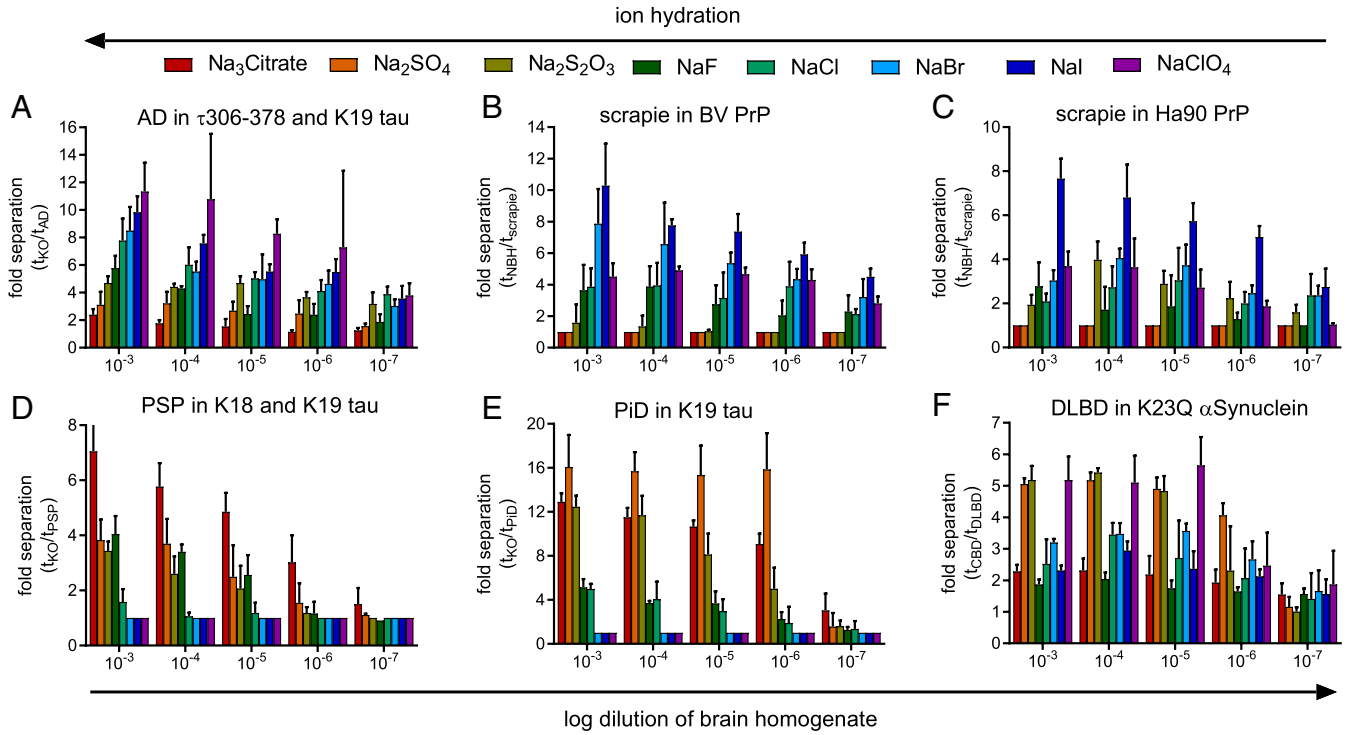

Fig. 4. Hofmeister effects on the fidelity of 6 amyloid seed-polymerization assays. Fidelity, quantified as fold separation, represents the mean time to threshold of a negative control (negative controls: for AD, PSP, and PiD: KO mouse BH; for scrapie: normal hamster BH; for DLBD: corticobasal degeneration BH) divided by the time to threshold fluorescence for 4 replicate reactions at a given dilution of BH. Assays in the presence of different salts in the Hofmeister differ in fidelity by up to a factor of 16. (*A*) AD in τ306–378 and K19 tau. (*B*) Scrapie in BV PrP. (*C*) Scrapie in Ha90 PrP. (*D*) PSP in K18 and K19 tau. (*E*) PiD in K19 tau. (*F*) DLBD in K23Q α-Syn.

Table 2. Relative seed concentrations measured in Hofmeister anions with 6 RT-QuIC assays

Brain seed (substrates)	$Na_3Citrate$	Na_2SO_4	$Na_2S_2O_3$	NaF	NaCl	NaBr	NaI	$NaClO_4$
	Measured seed concentrations in brain tissue (log SD_{50} per mg brain*)							
AD (τ306 + K19CFh)	6.25	6	8	5	9.25	9.25	10.5†	10
Scrapie (Ha90 PrP)	2.5	2.5	3.25	7	7.5	7.5	8.25	8.25
Scrapie (BV PrP)	2.5	2.5	8	5.5	7.75	8	8.5	7
PiD (K19CFh)	8.50	7.75	7.25	7.25	4.75	3.5	3.5	3.75
PSP (K18CFh + K19CFh)	7.5	7	6	6	3.5	2.5	2.5	2.5
DLBD (K23Q αSyn)	7	6.75	7	7.5†	6.75	6.75	6.5	7.5†

More sensitive

Less sensitive

*Spearman-Karber calculations of the log dilution of the designated brain tissue at which 2/4 reactions reached a ThT threshold above 100 × SD of the baseline fluorescence, prior to any spontaneous fibril formation in negative reactions.
†log SD_{50} calculations that are underestimates because the serial dilutions performed in the given condition did not reach end-point.

For example, NaI improved the sensitivity of the AD and prion RT-QuIC assays by at least 0.5 log in at least 2 determinations of SD_{50} concentrations. Similar log SD_{50} per milligram of brain determinations for the cationic series are summarized in *SI Appendix*, Table S3, indicating that the optimal cation depended on the RT-QuIC assay. Due to the weaker effects of cations relative to anions on fold separation and log SD_{50} per milligram of brain determinations, we decided to focus further optimization on modifying the anionic environment of the various QuIC reactions.

To further probe Hofmeister effects on tau RT-QuIC sensitivity, we tested 8 4R tauopathy brains (4 PSP, 3 corticobasal degeneration [CBD], and 1 argyrophilic grain disease [AGD]) in improved 4R RT-QuIC conditions that resulted from salt screening. Fig. 5 shows log SD_{50} concentrations of individual brains in 4R tau RT-QuIC assay conditions either in NaCl (not outlined) or in $Na_3Citrate$ (outlined). Sensitivity gains of up to a million-fold were obtained by using 300 mM $Na_3Citrate$ versus 300 mM NaCl. Arrows highlight the shift in log SD_{50}/mg brain tissue values obtained for identical brains assayed in NaCl (beginning of arrow) and $Na_3Citrate$ (point of arrow) at concentrations of 300 mM. The PSP BH assayed and described in Fig. 4*D* and Table 2 is circled in red. Certain AGD, CBD, and PSP cases gained up to 7, 5, and 4 logs of sensitivity, respectively. In contrast, little to no such gains in seeding activity were seen for 3R or 3R/4R tauopathy BHs or immunohistochemically tau-negative controls. To investigate if this sensitivity increase was due to the 6-fold ionic strength difference of 300 mM $Na_3Citrate$ (I = 1.8 M) compared to 300 mM NaCl (I = 0.3 M), we performed the 4R RT-QuIC in 4 salts with matching ionic strength (*SI Appendix*, Fig. S5). When ionic strength was normalized by comparing 300 mM $Na_3Citrate$, 1.8 M NaCl, 1.8 M NaI, or 450 mM Na_2SO_4 in the 4R RT-QuIC assay, the citrate-based assay still gave improved sensitivity over the NaCl-based assay, suggesting that the sensitivity gains with $Na_3Citrate$ were due in part to an ion-specific effect, rather than ionic strength alone. Analysis of additional 4R tauopathy brain and CSF specimens using 300 mM $Na_3Citrate$ will be described elsewhere (34).

Titration of Sodium Salts Enhanced Fidelity, Speed, and Sensitivity of 3 Tau Assays. To further optimize the 3R, 4R, and AD tau RT-QuIC assays, we assayed 10^{-3} to 10^{-10} dilutions of BH in increasing concentrations of the sodium salts of Hofmeister anions. Fig. 6*A* shows lag times for mock-seeded fibril formation in assays previously developed for AD (*Top*), PiD (*Middle*), and PSP (*Bottom*) tau seeds. At higher salt concentrations (>400 mM), the 3 tau assays followed the canonical series directly, such that mock-seeded fibrils were generated more quickly in $citrate^{3-} > SO_4^{2-} > \ldots > I^- \approx ClO_4^-$. However, at low concentrations (<100 mM) the series had inverted effects on mock-seeded tau fibril formation, in agreement with several studies observing an inversion of Hofmeister effects occurring at similar ion concentrations (24, 35–37). Despite these similarities in effects on mock-seeded tau-fragment fibrillization kinetics, the fold separation between seeded and mock-seeded lag phases (Fig. 6*B*) showed a trend of $citrate^{3-} < SO_4^{2-} < Cl^- < I^-$ for the AD assay and an inverse trend for the PiD and PSP assays. Complete fold-separation plots are shown in *SI Appendix*, Figs. S6–S9. Even when fold separations in the best-performing salt concentrations were compared at a single BH dilution (10^{-3}), the respective Hofmeister trends were apparent (Fig. 7*A*). We then calculated log SD_{50} concentrations for the best salt concentrations for 4 tau RT-QuIC assays (Fig. 7*B*), which correlated weakly, but significantly (R^2 = 0.44, P < 0.0001), to fold-separation values (Fig. 7*C*). The optimized AD assays [with τ306–378 + K19CFh as published (15), or with τ306–378 alone (modified)] each allowed detection of tau seeds in $\leq 10^{10}$-fold AD BH dilutions, while the PiD- and PSP-optimized assays were positive for 10^7- to 10^8-fold dilutions of the individual PiD and PSP BH samples that were tested (Fig. 7*B*).

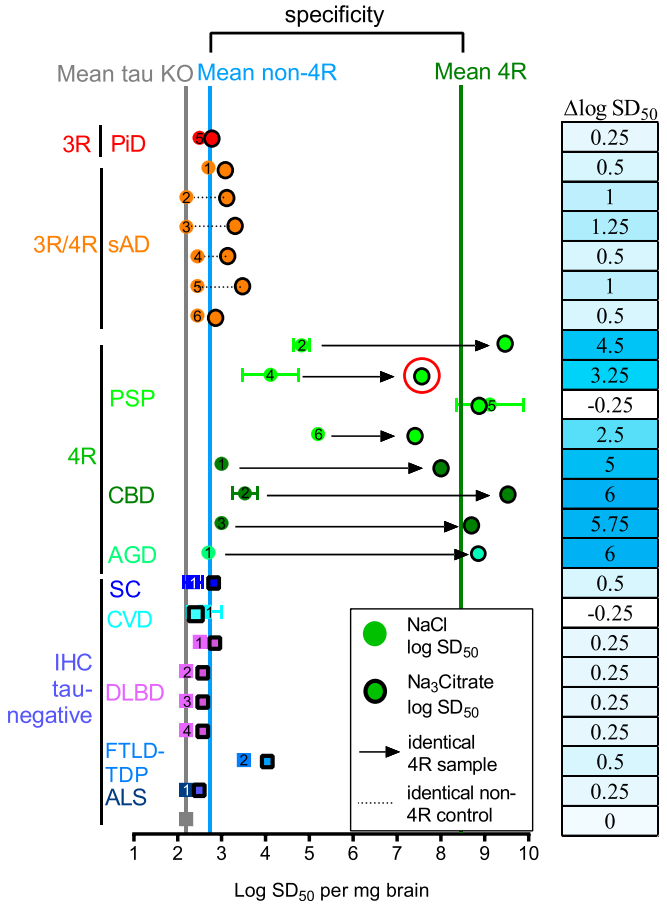

Fig. 5. $Na_3Citrate$ greatly enhanced the sensitivity of the 4R tau RT-QuIC without sacrificing specificity. Points represent log SD_{50}/mg brain tissue determinations for individual brains. Outlined points are in the presence of $Na_3Citrate$, compared to points without outline in the presence of NaCl. Numbers indicate different reported samples (10, 15). Arrows show the enhancement of sensitivity using single PSP, CBD, and AGD BHs. Dashed lines show the log SD_{50} of an identical BH in $Na_3Citrate$ (outlined) versus NaCl (not outlined). The adjacent table reports the numerical increase in log SD_{50} for each brain assayed. AGD, argyrophilic grain disease; ALS, amyotrophic lateral sclerosis; CBD, corticobasal degeneration; CVD, cerebrovascular disease; FTLD-TDP, frontotemporal lobar dementia with TDP43 positivity; sAD, sporadic AD; SC, senile change.

Hofmeister Effects Can Enhance Detection of Brain-Derived Seeds Spiked into Human Plasma. To test the impacts of salts on the detection of aggregates in diagnostically available biospecimens, we spiked 10^{-5} dilutions of AD or KO BH into pooled human plasma and analyzed them by AD tau RT-QuIC. Fig. 8*A* shows 10^{-5} AD-seeded lag times as they were affected by varying concentrations of human plasma, Na_2SO_4, NaCl, and NaI, in the presence of 6 μM τ306–378. Moving from the strongly hydrated anion SO_4^{2-} to the more weakly hydrated anions Cl^- and I^-, a more gradual dose–response of plasma components inhibiting AD-seeded fibril elongation was observed. The observed effects depended upon plasma concentration, with Na_2SO_4, NaCl, and NaI providing the best fold separation values in high-, medium-, or no-plasma conditions, respectively (Fig. 8*B*).

More Sensitive Detection of Human Sporadic Creutzfeldt–Jakob Disease Prion Seeds in Brain and Ante Mortem Nasal Brushings. After observing that Hofmeister effects could help overcome the inhibitory effects of human plasma components on RT-QuIC reactions, we explored the use of Hofmeister ions in detecting aggregates in diagnostically available sporadic Creutzfeldt–Jakob disease (sCJD) olfactory mucosae (OM). First, we compared Hofmeister anions from NaF to NaI on sCJD BH, which revealed an ∼100-fold increase in sensitivity for sCJD prion seeds in BHs in NaI relative to the NaCl used in second-generation RT-QuIC assays for human prions (9) (Fig. 9*A*). Specifically, in NaI, detection was lost at 10^{-9} to 10^{-10} dilutions of an sCJD brain, while in NaCl, detection was lost over 10^{-7} to 10^{-9} dilutions. In addition to improving sensitivity of sCJD prion detection, NaI improved the kinetic distinction of sCJD-seeded reactions from control NBH-seeded reactions (Fig. 9*B*), which is in agreement with the trends observed for scrapie-seeded reactions in Fig. 4. Because OM nasal brushings are easily obtained from living individuals and have been shown to be suitable specimens for the ante mortem diagnosis of sCJD (12, 13), we then tested if NaI could improve the detection of sCJD seeds in OM. Indeed, NaI improved the sensitivity of detection by ∼10-fold (Fig. 9 *C* and *D*). Importantly, this gain in analytical sensitivity has the potential to improve early diagnostic sensitivity for human prion diseases as well as the dynamic range over which prion seeds can be measured in patients' samples collected longitudinally in therapeutic trials.

Hofmeister Analysis Enhances Prion Detection in Ear Homogenates. Because NaI helped to improve the detection of sCJD prions in OM samples, we then analyzed ear homogenate samples from chronic wasting disease (CWD)-positive deer that might also be particularly useful diagnostically, but have so far been difficult to analyze. Fig. 10 summarizes lag-time plots for Ha90 PrP RT-QuIC reactions on ear homogenates from 5 CWD-negative and 5 CWD-positive deer confirmed by enzyme-linked immunosorbent assay (38) of retropharyngeal lymph node (RLN). Fig. 10 *A* and *B* show 100% diagnostic sensitivity and specificity of the PrP RT-QuIC conducted on RLN from 5 CWD-negative and CWD-positive deer in the presence of 300 mM NaCl or NaI. Fig. 10 *C* and *D* shows lag-time plots of RLN-matched ear homogenates assayed at 10^{-2} dilution in identical conditions to the RLN assay. By selecting a cutoff time before any negative well reached a ThT threshold of the mean baseline + 100 SDs, CWD seeds were detected at a sensitivity of 80% in 300 mM NaI versus a sensitivity of 45% in 300 mM NaCl, calculated from 20 individual reactions representing 5 deer (e.g., NaI sensitivity = 16 observed positive ear reactions/20 expected positive ear reactions = 80%).

Discussion

In order to develop highly sensitive diagnostic methods for neurodegenerative diseases, we have analyzed the effects of 15 different salts in the Hofmeister series on polymerization reactions seeded by disease-associated forms of tau, α-Syn, and PrP. This is compared to their corresponding effects on apparently spontaneous polymerization reactions that can eventually occur in mock-seeded reactions. When seeds are provided in the tissue sample, the fibrillization kinetics are determined primarily by elongation and secondary nucleation (39, 40). In the absence of seeds, substrate protein monomers must spontaneously form nuclei capable in turn of seeding fibril elongation. Although such primary nuclei can sometimes be as small as a protein monomer (41), they are typically found in the form of multimers. Spontaneous primary nucleation is typically slower than seeded elongation and secondary nucleation (39, 40). Our results indicate that measurements of this kinetic separation in the presence of ions of the Hofmeister series can increase the detection of specific types of disease-associated seeds by several orders of magnitude (Fig. 5).

With a better understanding of how Hofmeister salts affect RT-QuIC assays of brain samples, we considered how salt selection might improve seed detection in accessible diagnostic

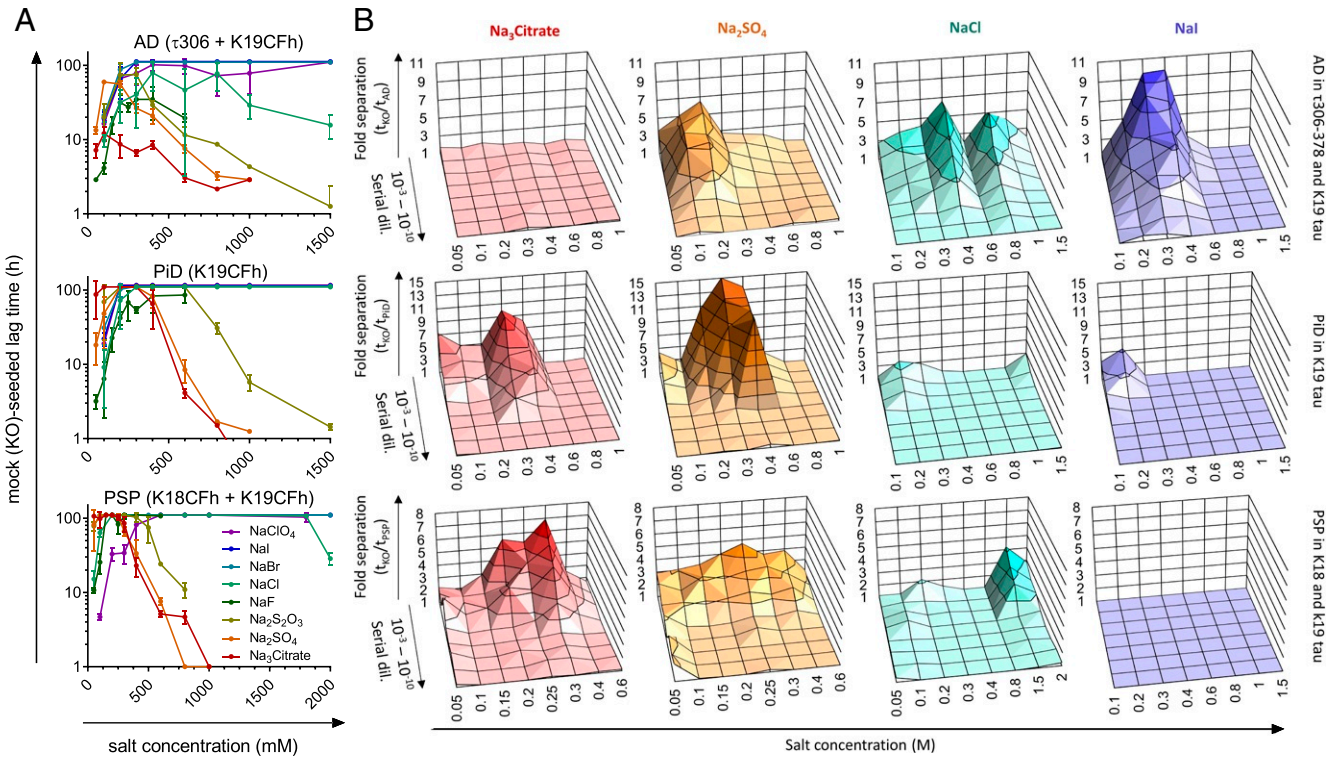

Fig. 6. Titration of Hofmeister anions in 3 tau assays. (*A*) Lag time of 4 replicate tau KO-seeded reactions in 3 tau assays over increasing sodium salt concentration. (*B*) Fold separation of KO versus AD (*Top*), KO versus PiD (*Middle*), and KO versus PSP (*Bottom*). The *z* axis represents 8 points for a reported salt concentration, where the value hugging the *y* axis (away from reader) is 10^{-3} dilution (dil.) of BH and the value hugging the x-axis (toward reader) is 10^{-10} dilution of BH.

biospecimens with typically lower seed concentrations. In the case of the AD tau assay, we have shown that inhibitory effects of plasma can also be overcome with strongly hydrated salts that tend to precipitate proteins (Fig. 8). While the AD tau seed detection in BH was enhanced in weakly hydrated anions, we observed a reversed effect in plasma, in which strongly hydrated SO_4^{2-} performed best. SO_4^{2-} and Cl^- both had optimal concentrations that maximized the kinetic separation between seeded and spontaneous fibrillization with a given dilution of plasma (Fig. 8, boxes). These data, taken together, emphasize the value of striking a balance between solubilizing and precipitating effects of reaction components, whether salts or sample matrix components.

While strongly hydrated ($Na_3Citrate$ and Na_2SO_4) precipitating salts improved the performance of the tau-based assays in matrices like plasma, these same salts completely inhibited the prion assays in matrices as dilute as 10^{-10} dilution of BH. By contrast, NaI, a weakly hydrated and solubilizing salt, improved the kinetic separation of prion-seeded from NBH-seeded reactions in 2 scrapie prion RT-QuIC assays. Further, this salt increased the analytical sensitivity in the detecting of human sCJD prion seeds in BH and nasal brushings by 6- to 32-fold. Such gains in analytical sensitivity for nasal brushings improves prospects for earlier diagnosis of human prion diseases, as well as the dynamic range over which prion seeds can be measured in patients' samples collected longitudinally in therapeutic trials. Also of practical utility is the improved detection of CWD prion seeds in deer-ear homogenates in NaI, raising the possibility that simple ear-punch biopsies might be used for ante mortem monitoring of this uncontrolled and rapidly spreading prion disease. The mechanistic basis for these effects of NaI is not clear, but, as they were seen with relatively concentrated and complex matrices (crude plasma, brain, and nasal brushings), it is possible that this solubilizing salt might act primarily by reducing inhibitory interactions of matrix components rather than directly altering the prion seeds or recombinant substrate proteins. Collectively, our experiments have shown that Hofmeister salt effects can be highly dependent on the sample matrix and recombinant protein substrates.

For researchers interested in pursuing seeded-polymerization assays, the correlation of fold separation at 10^{-3} dilution to measurements of assay sensitivity with end-point dilutions (i.e., measurements of log SD_{50}/mg tissue) suggest that choosing an initial reaction condition by maximizing kinetic separation of seeded versus spontaneous fibrillization at a single tissue dilution is likely to yield a more sensitive assay. Using this approach, one might more economically screen several conditions in a microwell plate at 10^{-3} dilution of on- and off-target BHs before performing more exhaustive end-point dilution comparisons.

Overall, our results demonstrate that, by controlling the physico-chemical factors that modulate the kinetics of seeded aggregation, it is possible to develop highly sensitive and highly specific detection methods that can provide opportunities for diagnostics of neurodegenerative disorders.

Materials and Methods

Preparation of the Recombinant Tau Constructs K18CFh, K19CFh, and τ306–378CFh. The tau constructs used in this work have all had cysteines modified to serines and with a C-terminal 6×His tag (CFh, cysteine-free, His tag). The purifications of K19CFh, K18CFh (34), and τ306–378CFh were conducted separately and followed described steps (10, 15). Tau substrates were cloned in the bacterial expression vector pET-28a, with N-terminal His tags and C322S and C291S mutations to prevent disulfide bond formation during purification and assay development. Expression followed the described overnight autoinduction steps (42). Recombinant substrate was purified over a 46 to 200 mM imidazole gradient over 8 His-trap 5-mL column

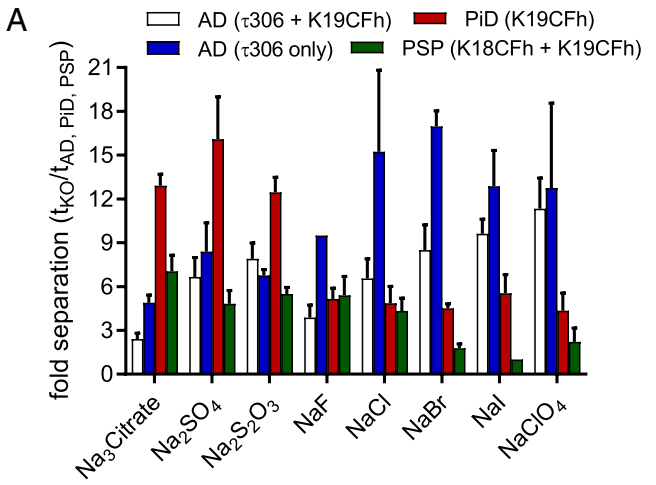

B

log SD50 determinations of best-performing salt concentrations by fold separation

	$Na_3Citrate$	Na_2SO_4	$Na_2S_2O_3$	NaF	NaCl	NaBr	NaI	$NaClO_4$
AD (τ306 + K19CFh)	3.5	8.5	8.5	6.25	9.25	9.25	10.5	7
AD (τ306)	6.5	9	9	9.75	9.5	9.75	9.75	10.5
PiD (K19CFh)	7.75	7.75	6.25	7.25	5.5	6.5	6.5	6.5
PSP (K18 + K19CFh)	7.5	7	7.25	7	6	3.5	3.5	4

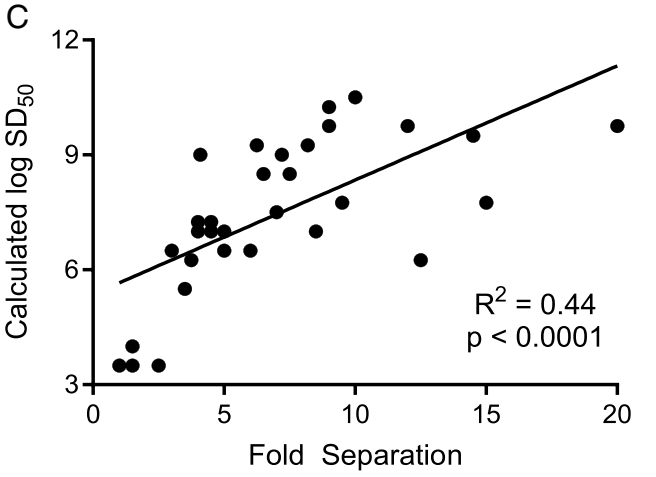

Fig. 7. Comparison of fidelity and sensitivity of the 3 tau assays with different salts in the Hofmeister series. (*A*) Maximum fidelity (in terms of fold separation) achieved using the different sodium salts. Surface plots of the titrations are shown in *SI Appendix*, Figs. S7–S10. (*B*) Comparison of the sensitivity (in terms of log SD_{50} values) at the best salt concentration reported in Fig. 8*A*. (*C*) Correlation of fidelity (fold separation) and sensitivity (log SD_{50} values). Data from all tau assays was grouped for correlation analysis (DFn = 1, DFd = 30; F = 23.11).

volumes (GE Healthcare). The substrate was precipitated in acetone overnight at 4 °C, followed by monomerization with 8 M Gdn·HCl and desalting by a PD-10 column (GE Healthcare). The substrate information is summarized in *SI Appendix*, Table S1.

Preparation of Recombinant α-Syn. The purification of α-Syn followed the steps described in ref. 7. The wild-type α-Syn sequence (GenBank accession no. NM000345.3) containing amino acids 1 to 140 with the K23Q mutation was ligated into the pET28 vector with N-terminal His-tag (EMD Biosciences) and transformed into BL21(DE3) *Escherichia coli*. Protein expression was performed by using the overnight autoinduction protocol described in ref. 42.

Preparation of Recombinant PrP. The purification of BV PrP followed the steps described in ref. 43, and Syrian hamster prion protein (Ha90 PrP) followed the steps described in ref. 32. In brief, PrP sequences encoding residues 23 to 231 of BV PrP with methionine at residue 109 and PrP sequences encoding residues 90 to 231 of Ha PrP were inserted into separate pET41 vectors. Vectors were transformed to Rosetta (DE3) *E. coli* and grown overnight with kanamycin and chloramphenicol. Expression was induced overnight by using the autoinduction system described in ref. 42 and purified from inclusion bodies in denaturing conditions with a nickel–nitrilotriacetic acid Superflow resin (Qiagen) on an AKTA fast protein liquid chromatograph. BV and Ha90 PrP were allowed to refold on the column in the presence of Gdn·HCl reduction gradient and eluted over imidazole gradient. The eluted protein was dialyzed into 10 mM Na_2HPO_4 buffer (pH 5.8), filtered through a 0.22-μm syringe filter, and stored at −80 °C for future use.

RT-QuIC Analysis of BH. Assay parameters for the 6 RT-QuIC assays are summarized in *SI Appendix*, Table S2, where asterisks denote parameters altered from published methods (7, 10, 31) to accommodate performance in 384-well plates. Assays previously performed in phosphate buffer were modified to Hepes buffer to avoid phosphate salt precipitation with Ca^{+2} and Mg^{+2} ions. In brief, each purified protein was thawed from −80 °C storage and filtered through a 100-kDa spin filter (Pall) in 500-μL increments. Protein concentration was adjusted and added to a premade master mix with buffer listed in *SI Appendix*, Table S2. In general, reaction mixes were prepared such that protein was added last and gently mixed in a pipetting boat. For all tau assays, 40 μM low-molecular-mass (5,500 kDa average) heparin was added to each master mix. To control for salt-induced pH changes, each salt stock solution was made in 10 mM Hepes and pH-adjusted to the final assay pH. A total of 49 μL of master mix was added to each well of a 384-well clear-bottom plate (Nunc). Serial dilution of BH occurred as follows: PiD and AD Tau assays: 10-fold dilutions in a background of 1× N2 supplement, 10 mM Hepes (pH 7.4), and 0.529% Tau KO mouse BH solution; PSP Tau assay: 10-fold dilutions in a background of 1× N2 supplement, 10 mM Hepes (pH 7.4), and 1.028% Tau KO mouse BH solution (2-fold KO concentration compared to PiD and AD assays); αSyn assay: 10-fold dilutions in a background of 1× N2 supplement and 10 mM Hepes (pH 8.0); PrP assays: 10-fold dilutions in a background of 0.05% (BV PrP) or 0.1% sodium dodecyl sulfate (SDS) (Ha90 PrP), 1× PBS, and 1× N2 supplement. BH dilutions were added to 384-well plates containing master mix in quadruplicate for each dilution and sealed with clear sealing tape (Nunc catalog no. 236366) and incubated (tau: 37 °C; αSyn and PrP: 42 °C) with 1-min cycles of revolution (tau: 500 rpm orbital; αSyn: 400 rpm orbital; PrP: 700 rpm double orbital) and 1-min cycles of rest, with ThT fluorescence read every 45 or 15 min (450 ± 10 nm excitation, 480 ± 10 nm emission, bottom read; BMG Fluostar).

For plasma-spiking experiments, a 10^{-3} AD BH and 10^{-3} KO BH were each spiked into aliquots of 0 to 20 to 40 to 60 to 80 to 100% plasma or CSF such that the final concentration of seeds was comparable to that in 10^{-5} BH. Pooled human ethylenediaminetetraacetic acid-treated plasma was purchased from Innova Research. Protein levels in each matrix were assessed by bicinchoninic acid assay (ThermoFisher). The reaction conditions were a modified AD tau RT-QuIC reaction using only 6 μM τ306–378, and run for 160 h of 1-min shaking, 500 rpm, orbital, 1-min rest, with ThT fluorescence reads every 15 min.

RT-QuIC Analysis of Deer-Ear Homogenate and Lymph Nodes. Ears and RLNs were collected from the severed heads of dead deer that had been harvested by licensed hunters. The deer were not killed for the purpose of supplying study materials, but, rather, as part of wildlife management practiced by the State of Colorado. The heads were submitted to us by individual hunters for CWD testing, and these extra tissue samples were collected opportunistically. As such, no animal-use-protocol approval was required. These tissue samples were homogenized in a bead beater to a 10% homogenate for storage at −80 °C for future use. Ear homogenates and lymph nodes were assayed at 1 and 0.1% concentration with 2 μL seeded into quadruplicate wells. Ear homogenate and lymph-node

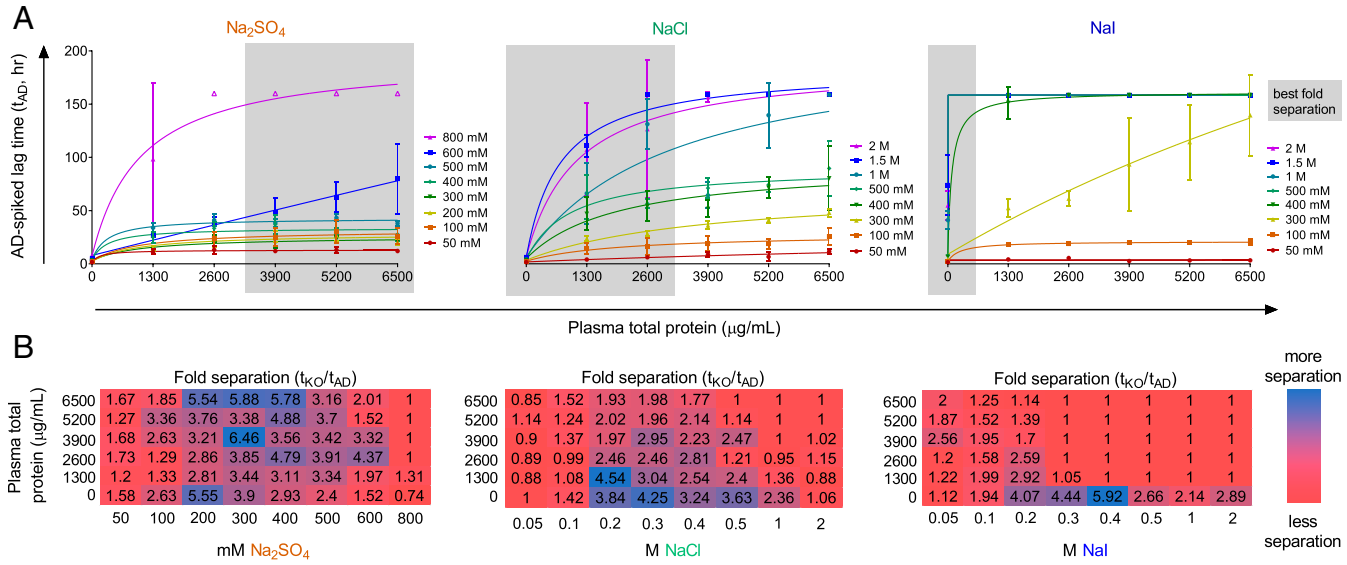

Fig. 8. Matrix inhibition by human plasma components in the AD tau RT-QuIC is overcome by Na_2SO_4. (*A*) Lag times of 1×10^{-5} AD-spiked human plasma with increasing concentrations of Na_2SO_4, NaCl, NaI, and human plasma. (*B*) Fold separation values calculated by dividing the KO-spiked spontaneous lag time by the AD-spiked lag time; blue boxes represent better kinetic discrimination between AD- and mock-seeded lag times.

CWD RT-QuIC buffer conditions were the same as described above for Ha90, with temperature increased to 50 °C, performed in 300 mM NaCl or NaI.

SD_{50} Analysis. SD_{50} values were calculated for individual BH serial dilutions by Spearman–Kärber analysis as described (33). Reported SD_{50} values represent the average of 2 experiments comprising 4 replicate reactions for

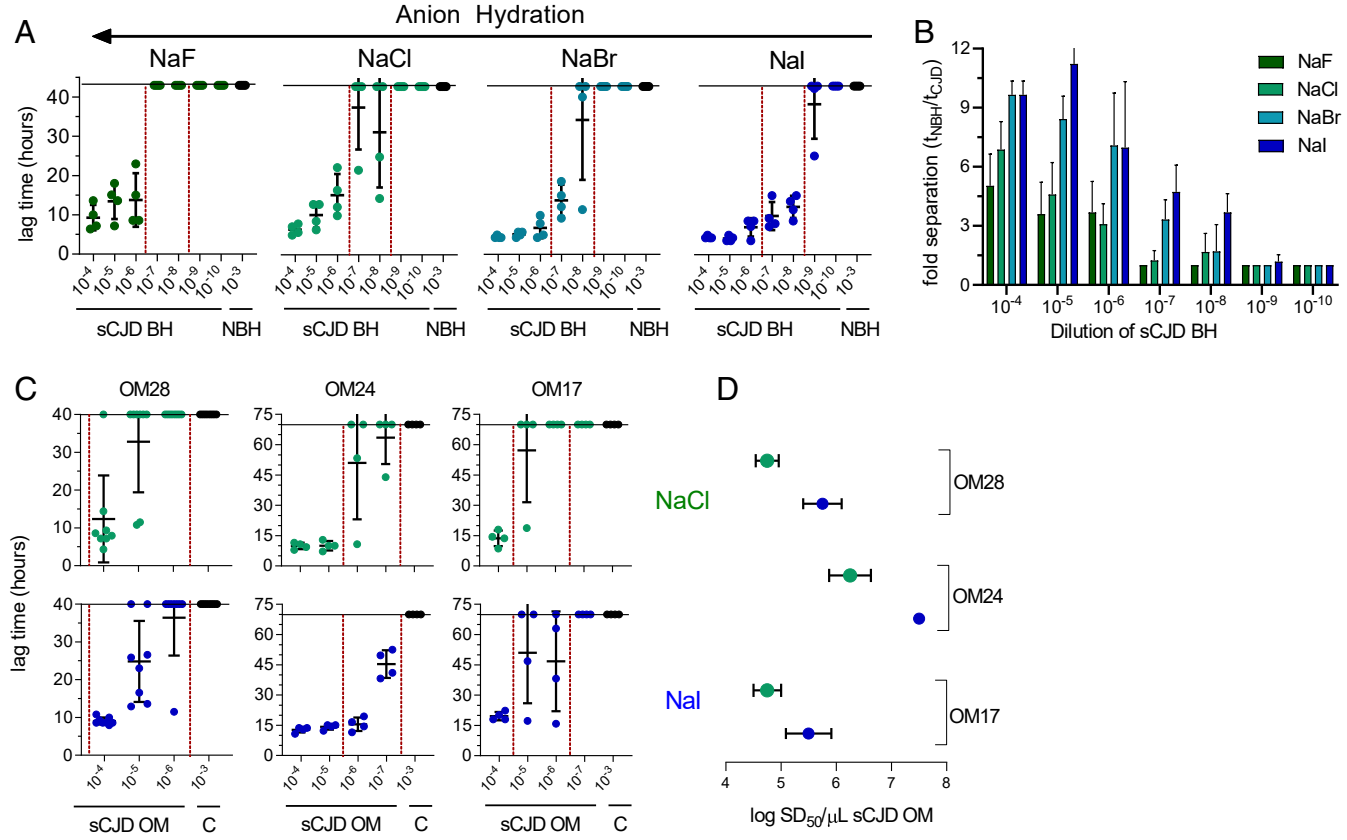

Fig. 9. Enhanced detection of sCJD prion seeds in BH and OM. (*A*) Lag-time data for serial dilutions of sCJD BH assayed with Ha90 RT-QuIC in 300 mM sodium salts of increasing anion hydration; horizontal lines denote the assay cutoff time determined by the occurrence of spontaneous (NBH-seeded) positive reactions; vertical dotted lines highlight dilutions showing the 10- to 100-fold increase in sensitivity in weakly hydrated anions. (*B*) Fold-separation values of the data presented in *A*. (*C*) Lag-time data for OM samples from 3 CJD patients and a nonneurological control (C) assayed in NaCl (*Upper*) or NaI (*Lower*); vertical dotted lines bracket dilutions showing the increased range of detection in NaI. (*D*) Log SD_{50} analysis of endpoint dilutions of ante mortem OM from sCJD patients in NaCl versus NaI; error bars represent SE calculated with the Spearman–Kärber method. Using this method, one of the OM24 data points was calculated to have an SE of zero.

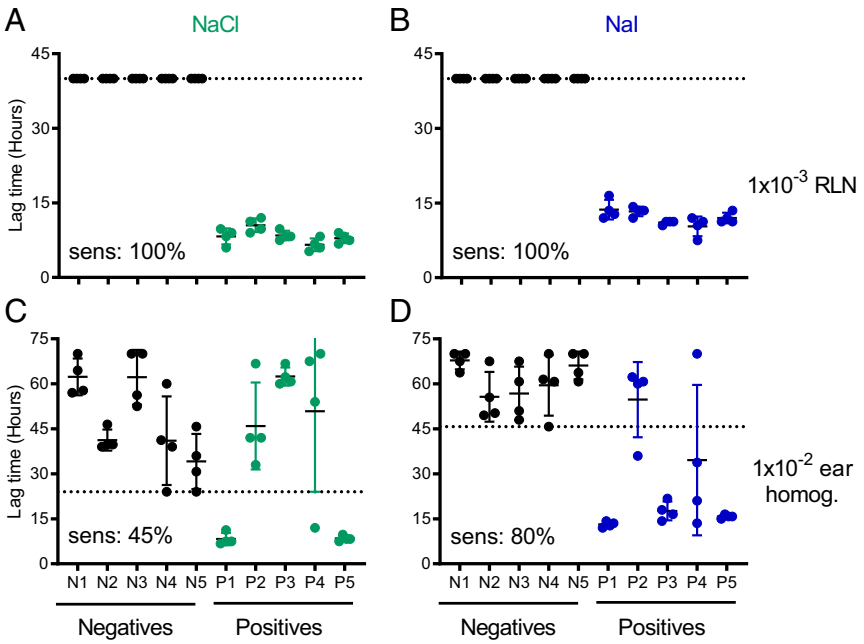

Fig. 10. Detection of CWD seeds in ear homogenates. (*A* and *B*) Lag-time data for Ha90 RT-QuIC on CWD-negative (N) and CWD-positive (P) deer retropharyngeal LN in NaCl (*A*) or NaI (*B*). (*C* and *D*) RT-QuIC analysis of matching ear homogenates at 10^{-2} dilution. Horizontal dotted lines denote the assay cutoff time determined by the occurrence of spontaneous (NBH-seeded) positive reactions.

a total of 8 replicate wells at each dilution. Because each salt affects the rate at which spontaneous fibril formation occurs, the cutoff value for SD_{50} calculations was the fluorescence read prior to the second replicate negative control well reaching fluorescence >100 × SD of the baseline fluorescence.

Brain Homogenization and Neuropathology. Human brain specimens were collected postmortem and sent deidentified to the National Institute of Allergy and Infectious Diseases (NIAID). All human brain samples assayed herein were prepared by homogenizing frontal cortex containing white and gray matter in 10% (wt/vol) homogenates in ice-cold phosphate-buffered saline (PBS) (pH 7.0) using a multibead shocker (Fisher). Homogenates were centrifuged at 2,000 × *g* for 2 min, with supernatants collected and aliquoted into 5- to 10-μL aliquots and stored at −80 °C until use. Human neuropathology samples from B.G. were handled as described (15). Brains used for each RT-QuIC are referenced in supplementary table 1 in refs. 10 and 15 and are as follows: AD tau RT-QuIC: sAD1; 3R tau RT-QuIC: PiD1 also used in refs. 10 and 15; αSyn RT-QuIC: DLBD1. For clarity, BHs used in 4R tau RT-QuIC are numbered in Fig. 5 and correspond directly to samples listed in supplementary table 1 in ref. 15. For hamster prion and normal hamster brain preparations, a half-brain was weighed and added to ice-cold PBS (pH 7.4) for a 10% (wt/vol) homogenization. Brains were homogenized by bead beating for 1 min (Biospec) and centrifuged at 2,000 × *g* for 2 min, and supernatants were removed, aliquoted at 7 μL, and stored at −80 °C until use. Hamster brains were collected under a protocol approved by the Rocky Mountain Laboratories Animal Care and Use Committee.

RT-QuIC Analysis of Nasal Brushings. Nasal brushings of the OM were collected from living patients as described (12). The study was approved by the ethics committee at Istituto Superiore di Sanità (Italy), which is recognized by the Office for Human Research Protections of the US Department of Health and Human Services. Informed consent for participation in research was obtained in accordance with the Declaration of Helsinki and the Additional Protocol to the Convention on Human Rights and Biomedicine, concerning Biomedical Research. The analyses of human specimens that were performed at the National Institute of Allergy and Infectious Diseases were performed under Exemption 11517 for the use of encoded samples from the National Institutes of Health Office of Human Subjects Research Protections. For RT-QuIC analysis, a disposable inoculating loop (Fisherbrand) was used to transfer ∼1 μL of the pellet into a tube with 25 μL of PBS. This suspension was sonicated until the pellet was dissolved, and then, a 10-fold dilution of this homogenate was made by using a 0.1% SDS/PBS/N2 solution as background. A total of 2 μL of the OM homogenates was seeded into a master mix containing 4 μM Ha90 PrP substrate, 300 mM salt, and 40 mM Hepes at pH 7.4, in quadruplicate reactions at each dilution. The plate was sealed with clear sealing tape (Nunc catalog no. 236366) and incubated at 50 °C, with 1-min cycles of shaking (700 rpm double orbital) and 1-min cycles of rest, with ThT fluorescence read every 45 min (450 ± 10-nm excitation, 480 ± 10-nm emission, bottom read; BMG Fluostar).

ACKNOWLEDGMENTS. We thank Drs. Gina MacDonald, Yanjie Zhang, Sue Priola, Ankit Srivastava, and Daniel Dulebohn for their helpful feedback and discussion that improved not only experimentation but also the readability of this manuscript; Nathan Winkelaar for custom Excel data-analytic software; and Ryan Kissinger for adeptly enhancing our schematics. This work was supported in part by the NIAID Intramural Research Program (B.C.). M.A.M. is supported by the NIH–Cambridge Scholars Program and the Cambridge Trust. E.S. is supported by UCB BioPharma, Japan Society for the Promotion of Science Fellowship for Japanese Biomedical and Behavioral Researchers at NIH. B.G. was supported by NIH Grant P30AG010133 and the Department of Pathology and Laboratory Medicine, Indiana University School of Medicine.

1. E. Grünblatt, Commonalities in the genetics of Alzheimer's disease and Parkinson's disease. *Expert Rev. Neurother.* **8**, 1865–1877 (2008).
2. Z. He *et al.*, Amyloid-β plaques enhance Alzheimer's brain tau-seeded pathologies by facilitating neuritic plaque tau aggregation. *Nat. Med.* **24**, 29–38 (2018).
3. D. A. Kocisko *et al.*, Cell-free formation of protease-resistant prion protein. *Nature* **370**, 471–474 (1994).
4. P. T. Lansbury Jr, Structural neurology: Are seeds at the root of neuronal degeneration? *Neuron* **19**, 1151–1154 (1997).
5. B. Caughey *et al.*, Amplified detection of prions and other amyloids by RT-QuIC in diagnostics and the evaluation of therapeutics and disinfectants. *Prog. Mol. Biol. Transl. Sci.* **150**, 375–388 (2017).
6. G. Fairfoul *et al.*, Alpha-synuclein RT-QuIC in the CSF of patients with alpha-synucleinopathies. *Ann. Clin. Transl. Neurol.* **3**, 812–818 (2016).
7. B. R. Groveman *et al.*, Rapid and ultra-sensitive quantitation of disease-associated alpha-synuclein seeds in brain and cerebrospinal fluid by alphasyn RT-QuIC. *Acta Neuropathol. Commun.* **6**, 7 (2018).
8. L. I. McGuire *et al.*, RT-QuIC analysis of cerebrospinal fluid in sporadic Creutzfeldt-Jakob disease. *Ann. Neurol.* **72**, 278–285 (2012).
9. C. D. Orru *et al.*, Rapid and sensitive RT-QuIC detection of human Creutzfeldt-Jakob disease using cerebrospinal fluid. *mBio* **6**, e02451–14 (2015).
10. E. Saijo *et al.*, Ultrasensitive and selective detection of 3-repeat tau seeding activity in Pick disease brain and cerebrospinal fluid. *Acta Neuropathol.* **133**, 751–765 (2017).

11. K. Sano *et al.*. Early detection of abnormal prion protein in genetic human prion diseases now possible using real-time QuiC assay. *PLoS One* **8**, e54915 (2013).
12. C. D. Orru *et al.*, A test for Creutzfeldt-Jakob disease using nasal brushings. *N. Engl. J. Med.* **371**, 519–529 (2014).
13. M. Bongianni *et al.*, Diagnosis of human prion disease using real-time quaking-induced conversion testing of olfactory mucosa and cerebrospinal fluid samples. *JAMA Neurol.* **74**, 155–162 (2017).
14. C. D. Orru *et al.*, Prion seeding activity and infectivity in skin samples from patients with sporadic Creutzfeldt-Jakob disease. *Sci. Transl. Med.* **9**, eaam7785 (2017).
15. A. Kraus *et al.*, Seeding selectivity and ultrasensitive detection of tau aggregate conformers of Alzheimer disease. *Acta Neuropathol.* **137**, 585–598 (2018).
16. C. D. Orru *et al.*, Factors that improve RT-QuIC detection of prion seeding activity. *Viruses* **8**, 140 (2016).
17. G. G. Tartaglia *et al.*, Prediction of aggregation-prone regions in structured proteins. *J. Mol. Biol.* **380**, 425–436 (2008).
18. K. Cheng *et al.*, Exploring physical and chemical factors influencing the properties of recombinant prion protein and the real-time quaking-induced conversion (RT-QuIC) assay. *PLoS One* **9**, e84812 (2014).
19. K. Sano *et al.*, Prion-like seeding of misfolded alpha-synuclein in the brains of dementia with Lewy body patients in RT-QuIC. *Mol. Neurobiol.* **55**, 3916–3930 (2018).
20. F. Hofmeister, Zur lehre von der wirkung der salze. *Archiv fur Exp. Pathol. Pharmakol.* **24**, 247–260 (1888).
21. Y. Zhang, P. S. Cremer, Interactions between macromolecules and ions: The Hofmeister series. *Curr. Opin. Chem. Biol.* **10**, 658–663 (2006).
22. Y. Zhang, P. S. Cremer, Chemistry of Hofmeister anions and osmolytes. *Annu. Rev. Phys. Chem.* **61**, 63–83 (2010).
23. H. I. Okur *et al.*, Beyond the Hofmeister series: Ion-specific effects on proteins and their biological functions. *J. Phys. Chem. B* **121**, 1997–2014 (2017).
24. Y. Zhang, P. S. Cremer, The inverse and direct Hofmeister series for lysozyme. *Proc. Natl. Acad. Sci. U.S.A.* **106**, 15249–15253 (2009).
25. B. A. Deyerle, Y. Zhang, Effects of Hofmeister anions on the aggregation behavior of PEO-PPO-PEO triblock copolymers. *Langmuir* **27**, 9203–9210 (2011).
26. L. M. Pegram, M. T. Record, Hofmeister salt effects on surface tension arise from partitioning of anions and cations between bulk water and the air-water interface. *J. Phys. Chem. B* **111**:5411–5417 (2007).
27. P. Jungwirth, D. J. Tobias, Specific ion effects at the air/water interface. *ACS Chem. Rev.* **106**, 1259–1281 (2006).
28. A. C. Apetri, W. K. Surewicz, Atypical effect of salts on the thermodynamic stability of human prion protein. *J. Biol. Chem.* **278**, 22187–22192 (2003).
29. L. A. Munishkina, J. Henriques, V. N. Uversky, A. Fink, Role of protein-water interactions and electrostatics in alpha-synuclein fibril formation. *Biochemistry* **43**, 3289–3300 (2004).
30. A. Sharma, S. H. Behrens, Y. O. Chernoff, A. S. Bommarius, Modulation of the formation of a β- and Sup35NM-based amyloids by complex interplay of specific and nonspecific ion effects. *J. Phys. Chem. B* **122**, 4972–4981 (2018).
31. C. D. Orru *et al.*, Bank vole prion protein as an apparently universal substrate for RT-QuIC-based detection and discrimination of prion strains. *PLoS Pathog.* **11**, e1004983 (2015).
32. J. M. Wilham *et al.*, Rapid end-point quantitation of prion seeding activity with sensitivity comparable to bioassays. *PLoS Pathog.* **6**, e1001217 (2010).
33. R. M. Dougherty, *Animal Virus Titration Techniques* (Academic Press, Inc., New York, 1964), pp. 183–186.
34. E. Saijo *et al.*, 4-repeat tau seeds and templating subtypes as brain and CSF biomarkers of frontotemporal lobar degeneration. *Acta Neuropathol.*, 10.1007/s00401-019-02080-2 (16 October 2019).
35. Y. V. Kalyuzhnyi, V. Vlachy, Explicit-water theory for the salt-specific effects and Hofmeister series in protein solutions. *J. Chem. Phys.* **144**, 215101 (2016).
36. A. Salis, F. Cugia, D. F. Parsons, B. W. Ninham, M. Monduzzi, Hofmeister series reversal for lysozyme by change in pH and salt concentration: Insights from electrophoretic mobility measurements. *Phys. Chem. Chem. Phys.* **14**, 4343–4346 (2012).
37. N. Schwierz, D. Horinek, R. R. Netz, Reversed anionic Hofmeister series: The interplay of surface charge and surface polarity. *Langmuir* **26**, 7370–7379 (2010).
38. N. J. Haley *et al.*, Detection of chronic wasting disease in the lymph nodes of free-ranging cervids by real-time quaking-induced conversion. *J. Clin. Microbiol.* **52**, 3237–3243 (2014).
39. J. H. Come, P. E. Fraser, P. T. Lansbury Jr, A kinetic model for amyloid formation in the prion diseases: Importance of seeding. *Proc. Natl. Acad. Sci. U.S.A.* **90**, 5959–5963 (1993).
40. T. P. J. Knowles *et al.*, An analytical solution to the kinetics of breakable filament assembly. *Science* **326**, 1533–1537 (2009).
41. K. W. Drombosky *et al.*, Mutational analysis implicates the amyloid fibril as the toxic entity in Huntington's disease. *Neurobiol. Dis.* **120**, 126–138 (2018).
42. B. G. Fox, P. G. Blommel, Autoinduction of protein expression. *Curr. Protoc. Protein Sci.* **56**, 5.23.1–5.23.18 (2009).
43. B. R. Groveman *et al.*, Charge neutralization of the central lysine cluster in prion protein (PrP) promotes PrP(Sc)-like folding of recombinant PrP amyloids. *J. Biol. Chem.* **290**, 1119–28 (2015).